

**MODELLING OF THE FRICTION WELDING PROCESS
BETWEEN MILD STEEL AND ALUMINA**

by

HAZMAN BIN SELI

**Thesis submitted in fulfillment of the requirements
for the degree of
Doctor of Philosophy**

June 2011

ACKNOWLEDGEMENTS

Praise be to Allah, the Cherisher and Sustainer of the worlds, for making this thesis a reality. I wish to express my heart feeling and profound gratitude to my supervisor, Prof Hj. Dr. Zainal Arifin Ahmad, for inspiring, motivating and guiding me to successfully complete my research work with full satisfaction. I also thank him for providing me with excellent research facilities and the numerous technical discussions which were invaluable for my research. I will forever cherish these three and a half years I spent at School of Materials and Mineral Resources Engineering (PPKBSM) with various valuable experience exposed from him.

I express great appreciation to Asc. Prof Dr. Ahmad Izani and Mr. Endri Rachman for their service on the co-supervision and their valuable suggestions for the thesis. I am also like to thank the School of Materials and Mineral Resources Engineering, the Dean Prof. Ahmad Fauzi Mohd Noor and academic, administrative as well as technical staff for providing the facilities and technical support.

Additionally, I would like to appreciate and thank Mr. Sharul Ami, Mr Suhaimi, Mr. Helmi, Mr. Farid, Mr. Khairi and Mr. Rashid who were more friends than fellow workers. They helped me with experimental setup and provided many valuable pointers for my research work during the innumerable discussions we had here. I would also like to thank all my colleagues at the PPKBSM making it a great place to work towards doctorate. I appreciate Mr. Nur Azam Badarulzaman, Dr Mohd Shah Rizal Kasim, Mr Nik Akmar, Mdm. Banjuraizah Johar, Mohd. Al Amin for their valuable suggestions in performing my PhD project.

I gratefully acknowledge the Ministry of Higher Education of Malaysia (MOHE) and Universiti Teknologi MARA (UiTM) for financially supporting me with a SLAI (Skim Latihan Akademik IPTA) scholarship and paid study leave respectively.

Last, but not least, I would like to thank my beloved wife, Salihah Ali, for her endless love and support or encouraging me in all my endeavors to this day. She was always there whenever I needed her and provided me with moral support during all my difficult times in this three and a half years PhD study.

TABLE OF CONTENTS

ACKNOWLEDGEMENTS	ii
TABLE OF CONTENTS	iv
LIST OF FIGURES	viii
LIST OF ABBREVIATIONS	xiii
LIST OF SYMBOLS	xvi
LIST OF APPENDICES	xxiv
LIST OF PUBLICATIONS AND SEMINARS	xxv
ABSTRAK	xxvi
ABSTRACT	xxviii

CHAPTER 1- INTRODUCTION

1.1 Overview of Ceramic/Metal Joining Process.....	1
1.2 Friction Welding Process and its Advantages.....	3
1.3 Overview of the rotary continuous direct drive FW	6
1.4 Problem Statement.....	9
1.5 Objectives of The Research	13
1.6 Research Approach and Methodology	13

CHAPTER 2- LITERATURE REVIEW

2.1 Introduction.....	16
2.2 Numerical Modelling.....	16
2.2.1 Basics of Numerical Modelling.....	18
2.2.2 Lagrangian and Eulerian Techniques	20
2.3 Modelling the FW Process.....	23
2.4 Realistic friction law for FW model	24
2.5 Thermal modelling and the input of heat	27
2.6 Analytical thermal models.....	29
2.7 Numerical thermal models.....	33

2.8	Modelling Mechanical Aspects of Friction Welding	39
2.9	Modelling of residual stresses	42
2.10	Modelling of Microstructure and validation	46
2.11	Other Related Process Models	47
2.11.1	Metal Forming Models	47
2.11.2	Friction Stir Welding Models	48

CHAPTER 3- MATHEMATICAL MODELS

3.1	Background	50
3.2	FD thermal model	51
3.2.1	Analytical frictional heat generation model	52
3.2.2	Plastic deformation heat source	54
3.2.3	Heat transfer	54
3.2.4	Explicit finite difference method	57
3.3	Diffusion couples	60
3.3.1	Instantaneous planar diffusion source in an infinite medium	60
3.3.2	Diffusion couple development	63
3.4	Thermo-mechanical FE model	66
3.4.1	Modeling Approach	67
3.4.2	Thermo-mechanical model	72
3.4.3	Finite Element Model	74
3.4.4	3-D local model based on material behavior and deformation analysis using explicit dynamics	76
3.4.5	Governing Equations for explicit dynamic analysis	78

CHAPTER 4- MATERIALS AND METHODS

4.1	General	84
4.2	Materials properties	84
4.3	Temperature measurement of FW Process	86
4.3.1	Sample preparation	86
4.3.2	Samples arrangement for temperature measurement	87
4.3.3	Temperature measurement setup	88

4.4	Computation of thermal FD and diffusion models	89
4.4.1	Writing codes for calculation	90
4.4.2	Input parameters for temperature calculation	93
4.4.3	Input parameters for concentration calculation	94
4.5	FE simulation of the FW process	95
4.5.1	Abaqus/CAE	96
4.5.2	Assumptions	100
4.5.3	Geometry and model	101
4.5.4	Input parameters for simulation	105
 CHAPTER 5- RESULTS AND DISCUSSION		107
5.1	Background	107
5.2	Intermediate layer condition	107
5.3	Temperature profiles of FD analysis	109
5.3.1	Heating Profile	109
5.3.2	Cooling Profile	113
5.3.3	Verification of FD model	114
5.4	Interfacial aluminum diffusion analysis	118
5.4.1	Aluminum diffusion across aluminum-alumina interface	118
5.4.2	Aluminum diffusion across aluminum-steel interface	122
5.5	Analysis of 3D FE process model of FW	126
5.5.1	Deformation of the interlayer	126
5.5.2	Temperature distribution	128
5.5.3	Strain and stress distribution	133
 CHAPTER 6-CONCLUSIONS AND RECOMMENDATIONS		
6.1	Conclusions	135
6.2	Recommendations	137
6.2.1	Modeling of the thermo-mechanical state and the material flow	137
6.2.2	Improving the experimental setup of the FW process	138
6.2.3	Microstructural analysis of weld	138
 REFERENCES		139

LIST OF TABLES

		PAGE
Table 4.1	Materials chemical composition from XRF analysis (Noh et al., 2008).	85
Table 4.2	Material properties of aluminum alloy 6061-T6 (Chao and Qi, 1998), alumina (Zimmerman et al., 2009) and steel (Maalekian et al., 2008).	85
Table 4.3	Input constant parameters used in simulation of 1D- FD thermal model of friction welding process.	93
Table 4.4	Input constant parameters used in concentration calculation of diffusion model.	95
Table 4.5	Friction welding condition for the process simulation.	106
Table 5.1 :	Percent differences of the numerical and measured temperature profiles at point combinations showed in Figure 5.5.	115
Table 5.2	Composition and crystal structures of intermetallic compounds of Fe-Al (Soundararajan, 2006)	124
Table 5.3	Series of temperature changes for the FE model of the 3D FW.	130

LIST OF FIGURES

		PAGE
Figure 1.1	Three variants of friction welding method: comparison of heat generation over interface for three types of friction welding is shown with black arrows (Maalekian, 2007).	4
Figure 1.2	Schematic variation of welding parameters with time for direct drive friction welding process (Maalekian, 2007).	6
Figure 1.3	Schematic representation of the FW process.	8
Figure 1.4	A: one specimen rotates and other is stationary where a metal interlayer is clamped at the rotating specimen and aligned facing the stationary specimen.; B: two specimens are brought together as axial force is applied and rubbing of faying interlayer surfaces heats specimen locally and upsetting starts; C: process is complete when rotation of one specimen stops and upsetting ceases.	9
Figure 1.5	Example of successful friction welded mild steel and alumina.	9
Figure 1.6	Flowchart for the overall study.	15
Figure 2.1	Eulerian and Lagrangian approaches to numerical modeling. Notice the material moves through the Eulerian mesh, and distorts the Lagrangian mesh (Oliphant, 2004).	21
Figure 2.2	a) Yield stress of 20G steel as a function of strain rate, b) Friction coefficient as a function of temperature at two pressures (a: 40 N/mm ² ; b: 60 N/mm ²). The continuous lines denote the relation used for the numerical simulation in section 2.4 (Sluzalec, 1990) .	25
Figure 2.3	(a) Characteristic temperature curves for direct drive welding for low power welding of 20G steel cylinders at different distances from the weld-line ($z = 0$); 1: analytical solution, 2: experiment; 3: numerical solution with temperature independent material properties; 4 with temperature dependent properties. (b) (Sluzalec, 1993) high power welding of AlCuMg ₂ -alloys welded under different conditions showing measured (dashed) and predicted (continuous) profiles (Midling and Grong, 1994).	31

Figure 2.4	Comparison of experimental measured (continuous) and numerically simulated (dashed) temperature profiles for an IN718 inertia weld for two axial distances from the weld-line (Balasubramanian et al., 1999a).	36
Figure 2.5	Peak temperature as a function from the weld-line attained in an RR1000 weld inertia welded tube wall for (a) low pressure (L) (b) medium (M~37% higher welding pressure) and (c) high (H~87% higher welding pressure) (Grant et al., 2008).	37
Figure 2.6 :	Temperature profile on the lateral surfaces of the friction welded aluminum-alumina (time of heating 0.45 s), solid line - numerical calculation, points - measured by the thermovisual method.	38
Figure 2.7	Diffusion profile curve in intermediate layer calculated by FEM and obtained during the experiment (Zimmerman et al., 2009).	40
Figure 2.8	Comparison of predicted peak temperatures and those inferred from the microstructural study as a function of distance from the weldline (Grant et al., 2008).	41
Figure 2.9	Contour plots of the measured (left hand side) and modelled (right hand side) stresses in the (a) hoop, (b) axial and (c) radial directions. All stresses are plotted in MPa. The typical accuracy of the stress characterisation by neutron diffraction was ± 70 MPa. (Grant et al., 2008).	43
Figure 2.10	a) dilatometry data for cooling of CMV steel and b) the predicted post-weld cooled von Mises stress distribution in a CMV steel after inertia welding with and without phase transformation (Bennett et al., 2007). The austenitised zone is shown highlighted (inset).	45
Figure 3.1	Friction interface sketch.	52
Figure 3.2	Boundary conditions used for the model.	56
Figure 3.3	Linear flow characteristics of an instantaneous source M released into surrounding semi-infinite media.	61
Figure 3.4	The expected diffusion couple in friction welded mild steel-alumina.	63

Figure 3.5	Classical diffusion couple. Here the left and right member initially have uniform compositions of C_l and C_r respectively. Top : Physical configuration; bottom: the couple represented as a continuous distribution of instantaneous source of strength dM . The variable for the field point, where composition is determined, is x , whereas the running coordinate \hat{x} designates the initial source location.	64
Figure 3.6	Boundary conditions applied on mild steel rod, alumina rod and aluminum sheet.	70
Figure 4.1	Prepared mild steel and alumina rods and aluminum sheet.	86
Figure 4.2	Folded aluminum sheet, sintered alumina with holes and glued locking pin.	87
Figure 4.3	Top : The thermocouple positions on the alumina rod. Bottom : Strong red plastic star cloth tape was used to firmly attach the thermocouple beads into the holes.	88
Figure 4.4 :	Experimental setup for temperature measurement during friction welding process. The inset shows closed-up thermocouple positions attached in holes of alumina rod.	89
Figure 4.5	Example of a MATLAB function file.	91
Figure 4.6	Example of the workspace of function file in the MATLAB editor.	91
Figure 4.7	Flowchart of the temperature and concentration calculations.	92
Figure 4.8	Field Emission Scanning Electron Microscopy machine.	94
Figure 4.9	Friction welding setup on a lathe machine.	96
Figure 4.10	Window of Abaqus/CAE version 6.8-1 for simulation process.	97
Figure 4.11	Flowchart of the fully coupled thermo-mechanical analysis.	99
Figure 4.12	Boundary conditions and cross-sectional view of the assembled components.	102
Figure 4.13	The FEM model and dimension of the workpieces assembly of friction welding process in Abaqus 6.8.	104

Figure 5.1 :	(a) Appearance of the successful friction weld during temperature measurement. (b) Optical micrograph (magnification of $\times 50$) of cross-section microstructure of a typical friction welded aluminum alloy sheet.	108
Figure 5.2	Heating temperature distribution in (a) mild steel side and (b) alumina side.	110
Figure 5.3	The heating temperature distribution of friction welding process up to 3.2s.	112
Figure 5.4	The cooling temperature distribution of friction welding process after 3.2s.	114
Figure 5.5	Time-temperature profile at distance of 5mm and 10mm from the weld interface for numerical and experimental data.	115
Figure 5.6	(a) The $62\mu\text{m}$ length tested zone across the aluminum-alumina interface. (b) Linear distribution of the chemical elements performed by EDX line scan analysis in the intermediate layer.	120
Figure 5.7	Diffusion profile curve ($D=0.2\times 10^{-13}\text{m}^2/\text{s}$) in intermediate layer of Aluminum-alumina calculated and obtained during the experiment.	121
Figure 5.8	(a) The $8.79\mu\text{m}$ length tested zone across the aluminum-mild steel interface. (b) Linear distribution of the chemical elements performed by EDX line scan analysis in the intermediate layer.	123
Figure 5.9	Fe-Al phase diagram(Kattner and Burton, 1993).	124
Figure 5.10	Diffusion profile curve ($D= 0.9\times 10^{-14}\text{m}^2/\text{s}$) in intermediate layer of mild steel-aluminum calculated by FD and obtained during the experiment.	125
Figure 5.11	Appearance of friction welded alumina-mild steel with aluminum alloy interlayer	126
Figure 5.12	Top : Total deformation of the interlayer due to the horizontal displacement under mechanical loading and rotation (900 rpm). Bottom : Cross section view of the interlayer deformation across Eulerian boundary.	127
Figure 5.13	Temperature at nodes 55, 239 and 245 on the alumina rubbing surface as a function of time during the entire process period.	131

Figure 5.14	Temperature at nodes 56, 245 and 250 on the tied mild steel-aluminum interface as a function of time during the entire process period.	132
Figure 5.15	Von Mises stress (top) and equivalent plastic strain (bottom) for the interlayer rubbing surface.	133

LIST OF ABBREVIATIONS

R & D	Research and Development
AA6061-T6	Aluminum alloy 6061-T6
CMV	Chromium, molybdenum, and vanadium
AISI	American Iron and Steel Institute
SAE	Society of Automotive Engineers
FD	Finite difference
FE	Finite element
FEM	Finite element Method
FV	Finite Volume
3D	Three dimensional
1D	One dimensional
FW	Friction welding
FSW	Friction stir welding
TMAZ	Thermomechanically affected zone
Al ₂ O ₃	Aluminum oxide
AlN	Aluminum Nitrate
SiC	Silicon Carbide
RFW	Rotary friction welding
DD-RFW	Direct drive rotational friction welding
IFW	Inertia friction welding
ALE	Arbitrary Lagrangian Eulerian
MATLAB	Matrix Laboratory (Mathworks, Inc.)

Abaqus	Software applications for finite element analysis and computer-aided engineering. The name of this software is derived from the Greek word, “abax” (ἄβαξ), meaning “board covered with sand”
DEFORM	Engineering software that enables designers to analyze metal forming, heat treatment, machining and mechanical joining processes on the computer rather than the shop floor using trial and error, and is a trade mark of Scientific Forming Technologies Corporation
ADINA	Automatic Dynamic Incremental Nonlinear Analysis
HAZ	Heat affected zone
FTCS	Forward time centered space
ODE	Ordinary differential equation
DOF	Degree of freedom
EDX	Energy Dispersive X-Ray
XRF	X-Ray Fluorescence Spectroscopy
CAE	Computer-Aided Engineering
C3D8RT	Coupled thermo-mechanical hexahedron element with eight nodes
RPM	Revolution per minute
Wt	Weight
C	Carbon
Si	Silicon
P	Phosphorous
S	Sulfur
Cr	Chromium
Mn	Manganese
Ni	Nickel

Al	Aluminum
Cu	Copper
Fe	Ferum
Ca	Calcium
Mg	Magnesium
Na	Sodium
Bal	Balance

LIST OF SYMBOLS

\bar{K}	rank two stiffness matrix dependent on the problem definition and material properties
\bar{U}	resultant displacement vector
\bar{F}	vector of known boundary conditions
u	variable of interest (eg. displacement, temperature etc)
v	velocity or speed
v_o	constant
λ_o	constant
ρ_o	constant
x	space or distance in x axis direction
k	space
μ_{fr}	friction coefficient
P	pressure
σ_N	normal stress
T	temperature
τ	shear stress
τ_y	shear yield stress
I	moment of inertia
q	heat input,
ω	rotational or angular velocity
r_o	radius of the work-piece
$\dot{\epsilon}_{eq}$	equivalent strain rate
σ_{eq}	equivalent stress

z	direction along the rotation z axis
c	specific heat capacity
ρ	density of material
m'	parameter of the process
h	surface film conductance
t	time
t_h	heating stage time
q_o	net power
t_s	steady state stage
T_{max}	maximum temperature
k'	thermal conductivity
Q	rate of volumetric heat generation
s	deviatoric stress tensor
$\dot{\epsilon}$,	deviatoric strain rate tensor
K_o	constant
m_s	strain rate sensitivity
r	radius
A	cross-sectional area
F	force
dF_f	differential frictional force
μ	friction coefficient
v_T	tangential velocity,
P_f	frictional heating power generation
\dot{q}	internal energy rate

$\bar{\sigma}$	equivalent stress,
$\dot{\bar{\epsilon}}$	equivalent strain rate and
β	thermal efficiency of plastic deformation
T_{amb}	ambient temperature
u_o	shortening velocity
p_r	perimeter of the rod
L	length of rod
t_h	heating or frictional time.
x_j	distance from left end of the joined rods,
t_c	cooling time,
k_s	thermal conductivity of the mild steel
k_a	thermal conductivity of the aluminium, respectively
T_s	temperature of the free surfaces of the mild steel
T_a	temperature of the free surfaces of the aluminium
T_n	last temperature profile from the previous heating stage
n	final time step
c_o	concentration
D	diffusivity
M	finite mass of diffusant
D_m	diffusivities of mild steel
D_a	diffusivities of alumina
C_l	initial uniform compositions of left member
C_r	initial uniform compositions of right member
\hat{x}	initial source location

C	concentration of element
erf	error function
div	divergence
grad	gradient
\dot{Q}	volumetric heat generation.
q_1	frictional heat generated at the contact surfaces
q_2	heat due to plastic deformation
η	inelastic heat fraction,
σ	stress,
$\dot{\varepsilon}^{pl}$	rate of plastic straining,
V	material volume.
q_s	heat into mild steel
q_a	heat into alumina
\mathcal{D}	domain
$\dot{\sigma}$	stress tensor
\dot{p}_v	volume force intensity
a	acceleration.
\tilde{C}	image function of C
P_o	constant
Q_o	constant
π	pi
ε'_{ij}	total strain
ε'_{eij}	elastic strain
ε'_{pij}	plastic strain

ε'_{Tij}	thermal strain
i	increment number (1,2,3....)
j	increment number (1,2,3....)
G	tangent modulus
K	compression modulus
E	elastic or Young's modulus
ν'	Poisson's ratio
ε'_T	thermal strain
α_T	thermal expansion coefficient
σ_Y	yield strength
$[K]$	coefficient matrix
$\{u\}$	displacement vector
$\{F^a\}$	applied load vector
$[K_{ke}^T]$	Jacobian matrix (tangent matrix),
k_{ce}	subscript representing the current equilibrium iteration
$\{F_{ke}^{nr}\}$	vector of restoring loads corresponding to element internal loads
$[C(T)]$	heat capacity matrix
$[N]$	shape function matrix
$[K(T)]$	the thermal conductivity matrix
$[B_T]$	matrix relating temperature gradient to nodal temperatures;
$\{T\}$	nodal temperature vector
$\{\dot{T}\}$	nodal temperature rate vector
$\{\dot{Q}\}$	thermal driving force vector.

$[K]$	stiffness matrix for the assembly of elements (i.e. the structure)
$[Ke]$	a sum of the element stiffness matrices
$[dP]$	structure displacements and structure displacement derivatives vector.
$[F]$	load matrix
$[Fe]$	sum of the element load vectors
$[B]$	matrix relating strains to nodal displacements;
$[D]$	thermoelastic-plastic stress-strain matrix;
C_T	coefficients that depend on temperature-dependent material properties;
M_T	coefficients that depend on temperature-dependent material properties;
$[d\varepsilon_T]$	thermal strain nodal vector
A_{mc}	material constants
B_{mc}	material constants
m_{mc}	material constants
n_{mc}	material constants
C_{mc}	material constants
ε_p	effective plastic strain
$\dot{\varepsilon}_p$	the plastic strain rates
$\dot{\varepsilon}_o$	normalizing strain rates (typically 1 s^{-1})
T_{melt}	melting point
\ddot{u}_i^N	acceleration component
N	node number
p_l	load

k_{sm}	stiffness matrix
\ddot{u}	acceleration vector
M_{mm}	mass matrix
K_{sm}	stiffness matrix
P_{lv}	total load vector
θ	temperature in the node N
S	applied nodal thermal source vector
C_{lc}	lumped capacitance matrix
B_c	conductance matrix
θ	internal flux vector
ω_{max}	highest frequency in the mechanical solution response system of equations
λ_{max}	largest eigenvalue in the thermal response solution system of equations.
L_{min}	dimension of the smallest element in the mesh
α	thermal diffusivity of the workpiece
c_d	dilational wave speed calculated
c_j	convective velocity
K	Kelvin
W	Watt
m	meter
J	Joule
kg	kilogram
MPa	Megapascal
GPa	Gigapascal

$^{\circ}\text{C}$	degree celcius
s^{-1}	per second
Γ	Heat Partition coefficient
K_i	Thermal conductance
β	Inelastic heat fraction
η	Friction energy transformed into heat
μm	micrometer

LIST OF APPENDICES

- A. The Calculation of Temperature Distribution using MATLAB Codes
- B. The Calculation of Al diffusion using MATLAB Codes
- C. An Example Abaqus Input File
- D. Front page of published papers

LIST OF PUBLICATIONS AND SEMINARS

1. Seli, H., Ismail, A. I. M., Rachman, E. & Ahmad, Z. A. (2010) Mechanical evaluation and thermal modelling of friction welding of mild steel and aluminium. *Journal of Materials Processing Technology*, 210, 1209-1216.
2. Seli, H., Noh, M. Z., Md. Ismail, A. I., Rachman, E. & Ahmad, Z. A. (2010) Characterization and thermal modelling of friction welded alumina-mild steel with the use of Al 1100 interlayer. *Journal of Alloys and Compounds*, 506, 703-709.
3. Seli, H., Ismail, A. I. M., Rachman, E. & Ahmad, Z. A. (2010) Temperature Modeling for Friction Welding Process Between Ceramic and Metal. In Proceeding of 12th INTERNATIONAL CERAMICS CONGRESS PART C, *Journal of Advances in Science and Technology Vol. 64 (2010) pp 115-124*
4. Seli, H., Md. Ismail, A. I., Rachman, E. & Ahmad, Z. A. (2008) Preliminary numerical solution of cooling temperature distribution of friction welding process. Seminar Kebangsaan Aplikasi Sains Dan Matematik 2008. Batu Pahat, Johor, Malaysia 24-25 November 2008
5. Seli, H., Md. Ismail, A. I., Rachman, E. & Ahmad, Z. A. (2009) Mathematical modeling for heating and cooling temperature distribution during friction welding process. 1st International Conference on Welding Technologies'09. Ankara, Turkey, 11-13 June 2009
6. Seli, H., Md. Ismail, A. I., Rachman, E. & Ahmad, Z. A. (2009) Temperature modeling and investigation of the welded interface in the process of mild steel-aluminium friction welding. 3rd Powder Metallurgy Symposium & Exhibition 2009. Kuala Lumpur, Malaysia, 12th – 13th August 2009
7. Seli, H., Md. Ismail, A. I., Rachman, E. & Ahmad, Z. A. (2009) Numerical modeling for heating and cooling temperature profiles during friction welding process. Simposium Kebangsaan Sains Matematik Ke-17 (SKSM KE-17). Melaka, Malaysia, 15-17 Disember 2009
8. Seli, H., Md. Ismail, A. I., Rachman, E. & Ahmad, Z. A. (2010) Temperature Modeling for Friction Welding Process Between Ceramic and Metal. 12th International Ceramics Congress (CIMTEC 2010). Montecatini Terme, Tuscany, Italy, 6 -18 June 2010.

PEMODELAN PROSES KIMPALAN GESERAN DI ANTARA KELULI LEMBUT DAN ALUMINA

ABSTRAK

Mekanisme pemindahan haba, resapan jisim dan terma-mekanikal dalam kimpalan geseran belum lagi difahami sepenuhnya. Dalam kimpalan geseran dua bahan yang berlainan, dua rod dikimpal bersama dengan memegang satu daripada rod tersebut secara berputar tetap sementara satu rod lagi di bawah pengaruh beban paksi yang menyebabkan haba geseran terhasil pada antara muka. Tesis ini melaporkan suatu kajian kelakuan terma, terma-mekanikal dan resapan jisim rod-rod terkimpal geseran alumina-keluli lembut melalui penggunaan kepingan antara lapisan aloi aluminium. Suatu siri pengukuran suhu dan analisis pengesanan garis serakan tenaga sinar-X (EDX) ke atas kepekatan unsur Al telah dijalankan berdekatan dan merentasi antara muka dan digabungkan dengan model terma, resapan dan terma-mekanikal untuk memperolehi parameter-parameter bahan. Kerja ini telah mendemonstrasikan perubahan ketara dalam profil-profil sejarah masa-suhu bagi rod alumina dan kandungan unsur Al merentasi antara muka alumina-aloi aluminium dan keluli lembut-aloi aluminium. Ikatan yang diperolehi adalah melalui penguncian antara muka dan pembentukan fasa antaralogam. Peramalan profil-profil terma bezaan terhingga (FD) dan resapan telah dibandingkan dengan data termokupel sebenar dan data analisis pengesanan garis serakan tenaga sinar-X masing-masing daripada kimpalan-kimpalan yang dijalankan dalam keadaan yang serupa dan telah menunjukkan persetujuan yang agak baik. Suatu simulasi awal telah dilakukan untuk meramal ubahbentuk, tegasan,

keterikan dan taburan suhu ketika operasi penyambungan dengan menggunakan gandingan sepenuhnya terma-mekanikal model FE. Logam aloi aluminum yang digeserkan telah disimulasi dengan menggunakan suatu model bahan keplastikan-visco Johnson–Cook fenomenalogikal, yang sesuai untuk bahan-bahan yang mengalami keterikan-keterikan besar, kadar-kadar keterikan yang tinggi dan suhu-suhu tinggi. Tegasan, keterikan dan ubahbentuk yang tertinggi didapati berada di antara kawasan terkesan haba kimpalan yang berhampiran dengan bahagian keliling permukaan geseran dan berpadanan dengan profil suhu tertinggi yang telah ditinjau. Meskipun kaedah-kaedah permodelan yang dicadangkan di dalam kajian ini tidak dapat menggantikan suatu analisis berangka yang lebih tepat tetapi model-model tersebut menyediakan panduan dalam pembangunan parameter kimpalan seperti kelajuan putaran, daya paksi, daya tempaan, masa pemanasan dan masa kimpalan, dan membenarkan pemahaman yang lebih baik bagi proses kimpalan geseran alumina-keluli lembut yang menggunakan kepingan aloi aluminum sebagai antara lapisan sambungan.

MODELLING OF THE FRICTION WELDING PROCESS BETWEEN MILD STEEL AND ALUMINA

ABSTRACT

The heat transfer, mass diffusion and thermo-mechanical mechanisms in friction welding (FW) are not fully understood. In friction welding of two dissimilar materials, two rods are welded together by holding one of them still rotated while the other under the influence of an axial load which creates frictional heat in the interface. This thesis reports a study of the thermal, thermo-mechanical and mass diffusive behaviors of friction welded alumina–mild steel rods with the use of aluminum alloy sheet as interlayer. A series of temperature measurement and energy dispersive X-Ray (EDX) line scan analysis for Al element concentration were carried out near and across the interfaces region and were combined with thermal, diffusion and 3D FEM thermo-mechanical models to acquire material parameters. This work demonstrated the significant change in time-temperature history profiles in alumina rod and the Al element content across the interfaces of alumina-aluminum alloy and steel- aluminum alloy. The bond was obtained through interfacial interlocking and narrow intermetallic phase formation. The finite difference (FD) thermal and diffusion profiles predictions were compared to actual thermocouple and EDX analysis data respectively from welds conducted under identical conditions and were shown to be in fair agreement. A preliminary simulation was made to predict the deformation, stress, strain and temperature distribution during the joining operation using a fully coupled thermo-mechanical FE model. The aluminum alloy metal

being rubbed was simulated using a phenomenological Johnson–Cook viscoplasticity material model, which suited for materials subjected to large strains, high strain rates and high temperatures. The highest stress, strain and deformation are found to be within the heat affected of the weld close to the periphery rubbing surface region and correspond to the highest temperature profiles observed. Even though the modeling methods proposed in this study cannot replace a more accurate numerical analysis, they do provide guidance in weld parameter development such as rotational speed, axial force, forging force, heating time and welding time, and allows better understanding of the friction welding process of alumina–mild steel rods with the use of aluminum alloy sheet as interlayer.

CHAPTER 1

INTRODUCTION

1.1 Overview of Ceramic/Metal Joining Process

Welding of ceramic and metal gives new attractive possibilities of application due to the fact that both materials have significantly different physical, chemical and mechanical properties (Nicholas, 1989). Selection of ceramic/metal combinations depends on the application requirements.

In recent years, ceramic materials have proved their efficiency as members of various metal combinations for many engineering applications due to their special properties. For instance, engineering ceramics are gradually becoming important materials in many industrial applications due to their superior properties such as high temperature performance and resistance against wear and corrosion. However, the poor ductility and formability of ceramics restrict their applications to special parts and subassemblies of structures (Kvernes, 1990). The utilization of bulk ceramics relies strongly on joining them to structural materials, especially metals. For example, ceramics may be the best choice for an engine, but it is difficult to make an entire engine of ceramics at present. Joining ceramics to metals has consequently worldwide become a challenging subject for R&D work (Eagar, 1987, Suganuma, 1990).

Ceramic/metal joints provide solutions for various applications (Ming-Fang et al., 1999). The potential can be exploited according to the requirement of industrial

products and the advances in joining techniques (Jun-qing et al., 2003, Martinelli and Drew, 1995). Depending on the material combinations and the joint requirements, joining ceramic/metal can be performed using various processes such as (Nicholas, 1990):

- Diffusion Bonding
- Brazing
- Glazing
- Adhesive Bonding
- Mechanical Attachment

Correct selection of joining processes can diversify joint applications to a large extent and determine the success of dissimilar material joining from both technical and economical standpoints.

Joining ceramics with ductile metal by friction welding (FW) (Ferne et al., 1991) process is another method which is adopted from metal joining. Dawes (2001), pointed out, that aluminum, which is easily deformed can be bonded to low density (open structure) ceramics, such as Al_2O_3 , AlN , and SiC . He also reported that two ceramic rods could be butt joined by rotary friction welding, using an aluminum interlayer. Jones (2003) presented in the Internet the video clip, which showed “aluminum conductors for microelectronic application being joined to an aluminum nitride substrate, using a mini friction welding machine”. Wlosinski et al. (2004) establish the welding technological parameters for bonding aluminum alloy 6061-T6

and ceramic Al_2O_3 as well as copper and Al_2O_3 . The friction welding technique is worth developing in regard to ceramics/metal joints because it is relatively easy to apply practically and does not require any special conditions (in comparison to other welding technologies, e.g. vacuum). In order to apply it commercially on the industrial scale it is necessary to know what kind of phenomena takes place during the whole process and intermediate layer creation. Analysis of these phenomena can be helpful in improving both the method and strength of the bonds.

1.2 Friction Welding Process and its Advantages

The role of friction in material joining techniques first became important with the development of friction welding in the early 1960's. Dickson and Bahrani (1975) gave an outline of the main types of the friction welding process describing the effect of the main process variables like the velocity of rubbing, the axial pressure, the welding time as well as the thermal and frictional material properties. Friction welding is a solid-state joining process that produces coalescence by heat developed between two surfaces by a mechanically induced rubbing motion, mostly of rotational nature (Spindler, 1994). The two surfaces are held together under pressure and due to the developed heating, a plasticized layer forms at the interface. After a predetermined time the rotation stops and the pressure is increased to facilitate forging of the heated metal.

Basically, there are three variants of friction welding: rotary, linear and orbital (Figure 1.1). Rotary friction welding (RFW) is the oldest and most popular method

where one component is rotated about its axis while the other remains stationary. Then the two components are brought together under friction pressure. Actually the coalescence of materials is obtained through the combined effects of pressure and relative motion of the two components, heating the joint interface and inducing plastic deformation (Ambroziak, 2002). The deformation allows physical mismatching or interlocking between the two faying surfaces where strong joint could be welded after the interface cools down. Depending on the manner by which rotational energy is converted into frictional heat, rotary friction welding can be divided into two major process variations: direct drive (continuous drive) and inertia drive (stored energy). The direct drive has been used commercially since the 1940s. It requires constant energy from a source for any desired duration. The inertia drive, which was developed in the early 1960s, uses the kinetic energy stored in a rotating flywheel (Olson et al., 1993).

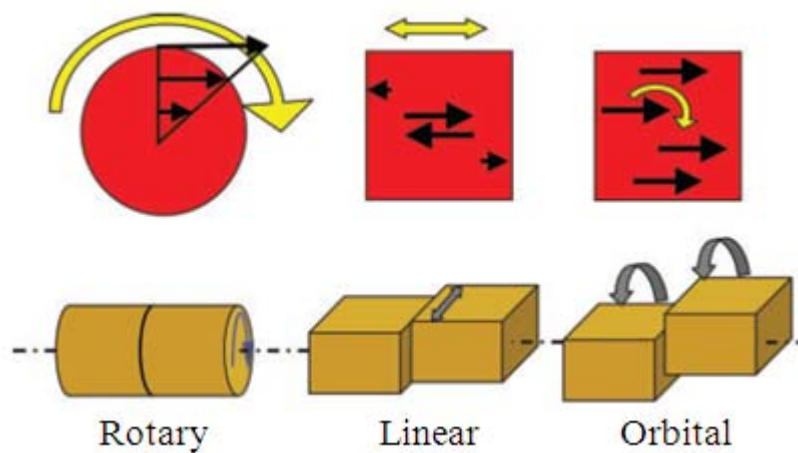


Figure 1.1 : Three variants of friction welding method: comparison of heat generation over interface for three types of friction welding is shown with black arrows (Maalekian, 2007).

The process advantages result from the fact that FW takes place in the solid state. Therefore, it is possible to join materials that are difficult to weld using conventional welding techniques. Friction welding can be used in existing and readily available machine-tool technology. The process is suitable for automation and robot use. Following are the most commonly cited advantages of the process which in turn drives the interest on the techniques (Ambroziak and Gul, 2007) :

- No filler wire
- No gas shielding for Al-alloys
- No welder certification
- Some tolerance of imperfect weld preparation (thin oxide layers can be accepted)
- Low distortion, even in long welds
- Excellent mechanical properties with forged quality where nearly 100% butt joint acquired at the contact area.
- Since there is no melting, no solidification defects occur, e.g. no segregation, slag inclusion, porosity and spatter
- Environmentally clean, no pollutants like smoke, fume or generated gases which need to be exhausted.
- Dissimilar metals can often be easily joined, even some considered incompatible or unweldable

On the other hand, the limitations of the FW process are:

- Workpieces must be rigidly clamped
- Components mostly limit to cylindrical or tubular shapes

1.3 Overview of the rotary continuous direct drive FW

The main variables in the rotary continuous direct drive friction welding process are rotational speed, axial force, burn-off, forging force, heating time and welding time (Lucas, 1971, Chandrasekaran et al., 1998, Grewe, 1997). These variables determine the amount of energy input to the weld and the rate of heat generation at the interface. It is to be noted that the rate of heat generation is not constant across the interface and that it also varies during the different phases of the welding cycle. During welding, axial shortening (also called upset, burn-off or axial displacement) and resisting torque of friction undergo changes. The relationship of friction welding parameter characteristics is shown in Figure 1.2.

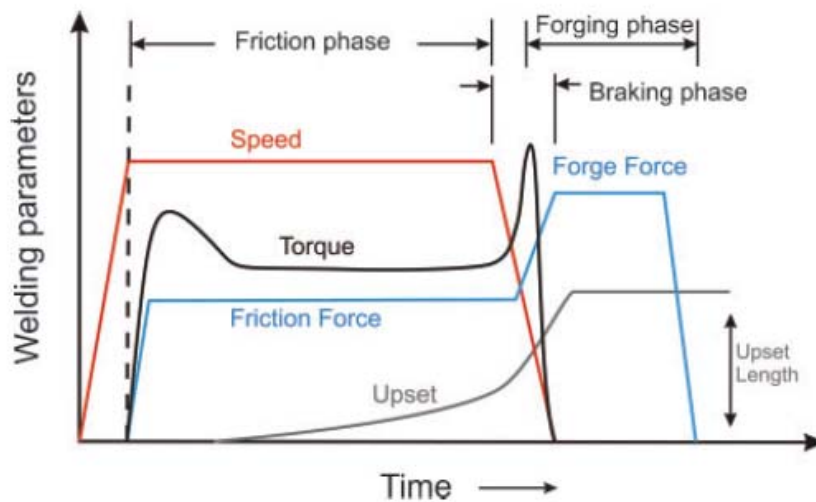


Figure 1.2 : Schematic variation of welding parameters with time for direct drive friction welding process (Maalekian, 2007).

According to the shape of the friction torque curve, the process can be divided into three phases (Olson et al., 1993). In the initial phase, the torque rises rapidly to a peak value after the start of the process. It then decreases gradually to the equilibrium value. The rapid rise and gradual fall of torque are associated with the interlocking

and breaking of asperities and subsequent softening of the material at the faying surfaces by frictional heating. Friction torque remains somewhat constant in the second phase, indicating that the process reaches a balance between strain rate hardening and temperature softening. Forging takes place in the third phase, which starts at the time of braking. Spindle rotation is immediately retarded, and the deceleration depends on the braking time. Axial force in this phase is usually increased to effect forging. The friction torque again rises after the onset of this phase, reaching another peak before sharply falling off to zero. This peak varies with deceleration and applied axial force. Under some circumstances, this final peak can be omitted by delaying the onset of the forging force. In direct drive friction welding, more frequently two stage friction force is applied; however, one stage friction force is sometimes used, especially in research work.

For metal (mild steel) and ceramic (alumina) joining process, the basic principle of rotary friction welding is modified by Noh et al. (2008) where a ductile metal (aluminum alloy) interlayer (bonding agent) is placed between the two faying surfaces as illustrated in Figure 1.3. In the continuous drive process one of the components is held stationary while the other is rotated at a constant speed.

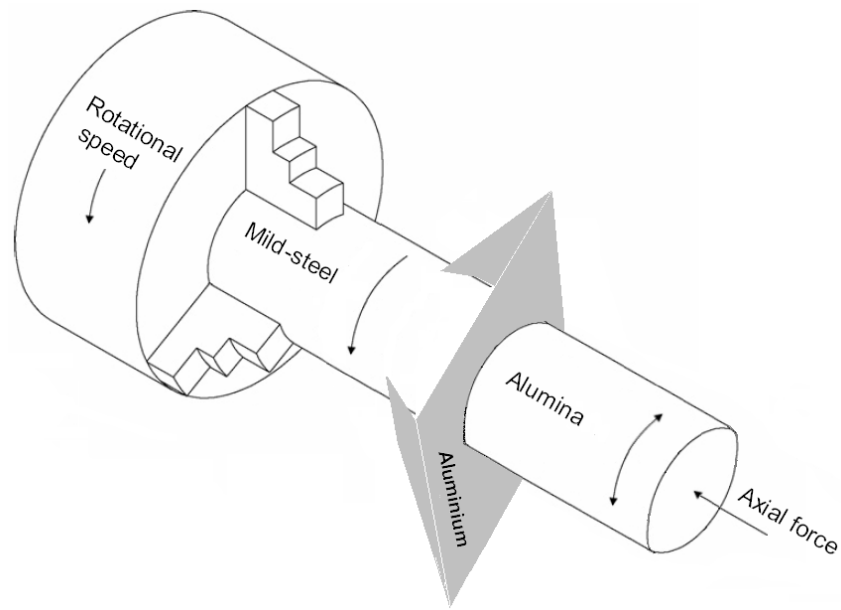


Figure 1.3 : Schematic representation of the FW process.

As illustrated further in Figure 1.4, the friction force is then applied as axial loading starts from the stationary component. It makes the two components rubbing against each other. When a predetermined weld time or amount of axial shortening is reached, the drive is disengaged to stop the rotating component. The axial force is maintained or increased until the weld has cooled down to ambient temperature. Then the excess aluminum plate is taken out of the interface and the metal-ceramic joint is ready for application as shown in Figure 1.5.

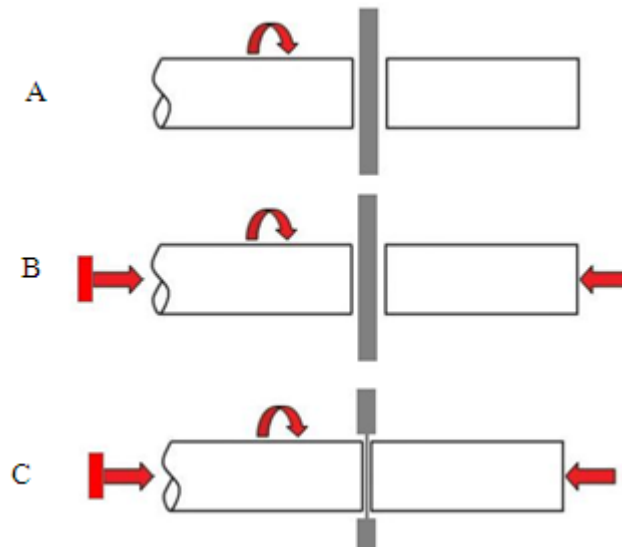


Figure 1.4 : A: one specimen rotates and other is stationary where a metal interlayer is clamped at the rotating specimen and aligned facing the stationary specimen.; B: two specimens are brought together as axial force is applied and rubbing of faying interlayer surfaces heats specimen locally and upsetting starts; C: process is complete when rotation of one specimen stops and upsetting ceases.



Figure 1.5 : Example of successful friction welded mild steel and alumina.

1.4 Problem Statement

Friction welding (FW) has opened up the horizon to join dissimilar materials that are impossible or difficult to be done by conventional welding methods. The applications of FW fall into a wide range of industries from agricultural, automotive

and aerospace to petroleum and electrical industries. It can produce components ranging from simple butt joints of drive shafts and oil drilling pipes to complicated or critical aircraft engine components. Gears, engine valves, axels in automotive industry, hydraulic piston rods and track rollers in agricultural industry, joining of turbine blades to discs in aircraft industry and electric motor shafts in power plant industry are some examples of FW applications.

Although extensive work with FW has been done on many materials, the metal and ceramic friction welding process with the use of soft metal interlayer is not yet covered fully. The friction welded ceramic-metal joint with the soft metal joining interlayer has been successfully produced by Noh et al. (2008). The mechanical mixing and forging force create the joints between the intermediate interlayer, ceramic and metal. Like other techniques of friction welding reported in many literature, the welding parameters (axial loading, rotational velocity and forging force) and the characteristics of the materials being joined with this method have effects on the temperature distribution, thermo-mechanical fields and the mass diffusion behavior that take place during the process. Therefore, being able to model and simulate the temperature distribution, thermo-mechanical fields and the mass diffusion in a friction weld will help optimizing the welding parameters to produce a high-quality weld. Investigation of these aspects could be performed either by experimentation or computer modeling. Normally the conduction of the experiments is very costly and time-consuming. Moreover, only a couple of points in the region

of interest are available for experimental measurement and acquired data for experimental analysis are very limited.

Compared to experimentation, modeling can be very useful because it can provide a convenient and straightforward way to vary material properties over a wide range and the analysis also provides direct information of temperature profiles and thermo-mechanical properties, avoiding or minimizing trial and error. Modeling of the process can play a key role in accelerating process development and reducing experimental costs. While the number of materials that can be welded to good quality by FW are increasing, fully comprehensive modeling of the process will take its place as a major development tool alongside experimental tests, reducing the amount of time and resources required for full experimental trials, enabling further improvement of the process and allowing friction welding to reach its full potential.

Modeling of the FW process has been addressed analytically and computationally from three different perspectives i.e. thermal modeling to predict temperature and heat transfer, solid mechanics based microstructure and material flow modeling and fluid mechanics based material flow modeling. Most of the models available in literature are focus on FW of similar and dissimilar metals. Only Zimmerman (2006) used FW method to join alumina and aluminum rod. He also developed models of the joining process. Modeling of FW process with the incorporation of aluminum bonding interlayer in Noh et al. (2008) work has not yet covered in this literature.

In this research, based on the modified FW process of Noh et al. (2008), three models are presented for the process. The first preliminary work is on modeling of 1D FD temperature distribution based on non-steady equation of Fourier's heat conduction with analytical frictional heat deduction. The second work is modeling on analytical mass diffusion profile at the interface of the weld. The last one is modeling and simulation of 3D FE coupled thermo-mechanical FW process model based on coefficient of friction. This friction based model depends on coefficients of friction adopted from the relevant literature. The soft metal interlayer material behavior is considered in the Johnson–Cook model constitutive relation. The heat generated during FW process is thought to be a combination of frictional heating and plastic deformational heating. It is likely that frictional heating represents the true physics of heat transfer as the interlayer material is plastically deformed between the two workpieces. By the use of these methods, the FW process is simulated and the shortcomings in the friction weld are described.

1.5 Objectives of The Research

This work has the following three aims:

- To develop a 1D FD thermal model for predicting heat generated at the rubbing surfaces by comparing the numerical and experimental data.
- To develop mass diffusion model for explaining the diffusion phenomena at the joint interfaces.
- To preliminarily develop a fully coupled thermo-mechanical 3D FE model and to predict the deformations, stresses, strain, and temperature distribution during the FW process.

To achieve these objectives, the FW process for the weld of steel and alumina rods with aluminum alloy interlayer is chosen following Noh et. al. (2008) work for the numerical models. The FD thermal model is simulated through software MATLAB 7 while the FE process model simulations are based on solid mechanics finite element formulations and carried out using the general purpose software Abaqus 6.8 (Theoretical Manual and User's Manual). The ultimate goal of this work is to apply such models to optimize the process parameters for FW of ceramic/metal joining with the use of ductile metal interlayer.

1.6 Research Approach and Methodology

The scope of this investigation is numerical simulation based on experimental recorded data. Although the FW technique itself is experimental in nature, development of the numerical model is directly related to the experimental results

and so the two are not altogether separable. As a result, the experimental information recorded provides the necessary information for construction of the numerical models. During the FW process, the welding parameters such as flywheel rotation speed, and axial forces are varied while the friction time and the temperatures at different places in the workpiece are recorded. These output variables help to study the thermal and mechanical response of the material during the weld formation process. Also, the cross-sections of the weld are cut and polished to determine mass diffusion in the parent materials.

The scope of the numerical portion of this study is to develop models that can simulate and analyze the actual weld formation process. This will help not only in better understanding of the process but also in selection of the process parameters and predicting the resultant weld quality. The soft metal interlayer undergoes large deformation under high stress and temperature. The thermal model will have to predict the accurate temperature distribution of the workpiece and this will determine the mass diffusion of the material that affects the actual weld formation.

Figure 1.6 shows the flowchart of the overall methodology used in this analysis. The main parts of this analysis are heat input prediction, finite element analysis, rotational speed measurement and temperature measurement. The prediction of heat input of 1D finite difference thermal model and mass diffusion profile is made through MATLAB 7 codes. The 3D finite element model is simulated and analyzed using ABAQUS 6.8 software.

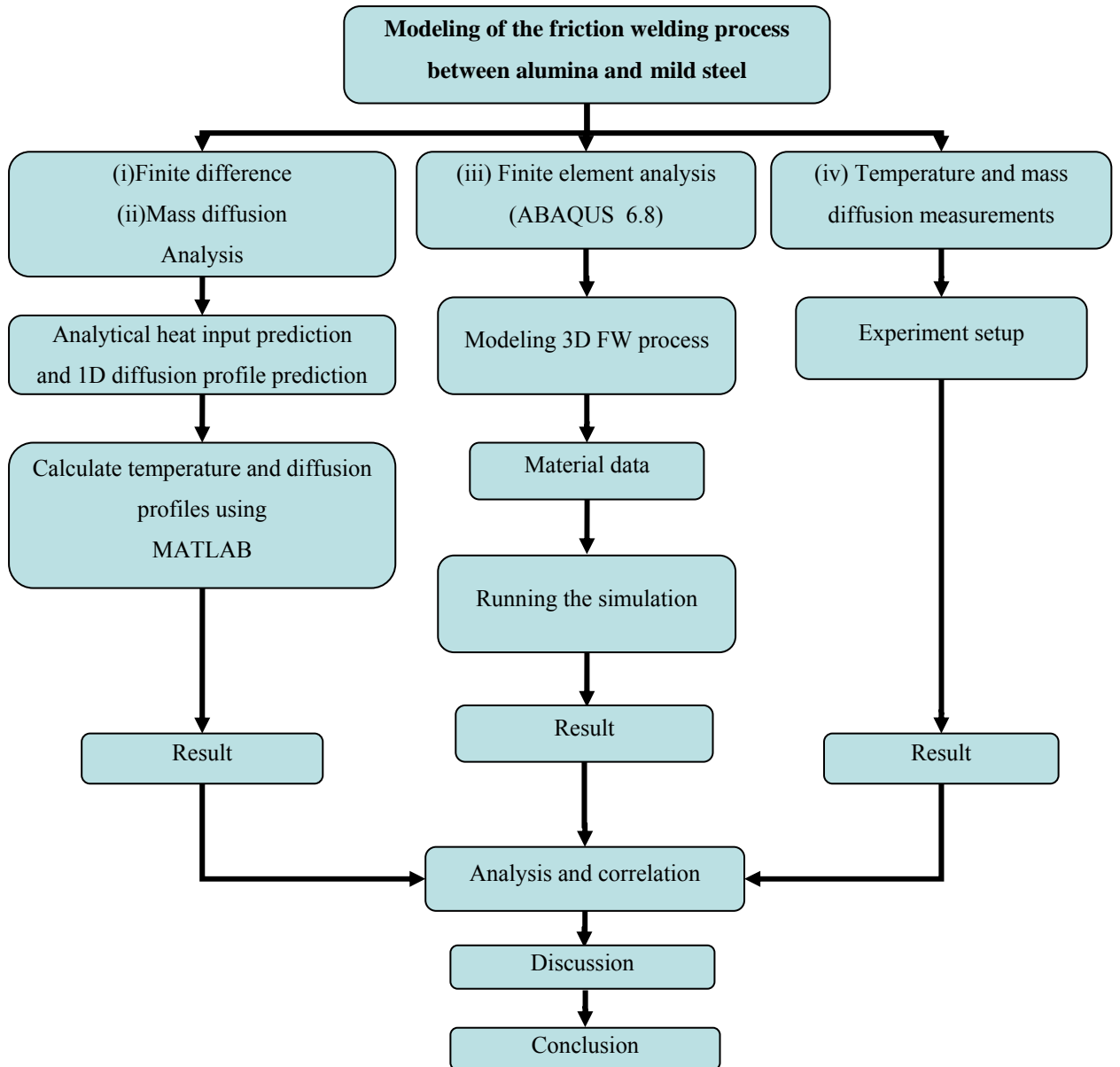


Figure 1.6 : Flowchart for the overall study.

CHAPTER 2

LITERATURE REVIEW

2.1 Introduction

There have been significant experimental investigations into FW of dissimilar materials ever since its invention; but computational modeling efforts to simulate the welding process are more recent. With growing interest in the process modelling of FW at numerous academics and research organizations, more and more literature is surfacing lately.

There are three broad categories in the modelling works i.e. thermal modeling to predict temperature and heat transfer, solid mechanics based microstructure modelling and fluid mechanics based material flow modelling. While the need for a unified approach towards all these models is universally acknowledged, not much success has been reported towards this end because of the extreme difficulty in modeling the FW process in a coupled and realistic 3D formulation. In the following, the current literature on FW is reviewed, with a consideration of efforts in several areas, including friction model, thermal modelling, residual stress modelling, material flow modelling and friction weld microstructure modelling.

2.2 Numerical Modelling

Most problems governed by differential equations can be solved by approximating the problem with a numerical method, and formulating a solution based on that method. Simplistically, numerical modelling is the division of a

geometrical domain into a finite number of nodal points and elemental volumes, the approximation of the governing boundary physics affecting each nodal point and its neighboring points, and the solution of the system of equations resulting from this approximation.

The modeling method an analyst may choose depends greatly on the definition of the problem. If a problem can be quantified mathematically, someone somewhere has numerically modelled a solution. However, inherent errors in the solution, the selection of simplifying assumptions, and the implementation of boundary conditions requires a foundation of experience and knowledge by the analyst. Numerical modeling applications might include, but are not limited to, the modeling of fluid motion, heat transfer, deformation of solids, coupled mechanical/chemical/electrical/thermal, wave formation and propagation, as well as macro or microscopic modelling. Each of these problem areas also has multiple solution methods. The challenge of selecting an appropriate numerical solution method starts with a definition of the problem. Static structures, for example, experience stress distributions throughout their members under normal loading conditions. An analyst seeking to characterize these stress distributions might choose a linear finite element method, a popular and generic choice in modern industry.

The FW process incorporates a challenging set of physical phenomena. These phenomena include: very large non-linear material deformations, highly temperature dependent material properties, and thermal heating from coupled frictional and

mechanical shear deformation. Therefore, a careful study of numerical modelling approaches must be conducted to properly select the appropriate method of analysis.

2.2.1 Basics of Numerical Modelling

There are three primary approaches to numerical modelling. The Finite Element, Finite Difference, and Finite Volume approaches all present modeling strengths and weaknesses to the analyst.

2.2.1.1 Finite Element Method.

The Finite Element (FE) approach is a widely popular choice due to its generic formulation, a technique that lends itself to commercial code production. The nodal points and elemental volumes are generically formulated to accommodate a wide range of problems. Integration of the governing differential equations is usually accomplished by a fully algebraic approach called Gaussian Quadrature. This integration approach, coupled with generic nodal and elemental volumes lends itself to generalized code production. The FE approach can be used for irrotational material advection, thermal diffusion, small and large displacements of solid materials, electricity and magnetism, and wave propagation.

$$\bar{K}\bar{U} = \bar{F} \tag{2.1}$$

The basic equation of the Finite Element method is shown here in equation 2.1, where \bar{K} is a rank two stiffness matrix dependent on the problem definition and material properties, \bar{U} is the resultant displacement vector, and \bar{F} is a vector of known boundary conditions (Balling, 2003). The FE approach is usually not the

method of choice for analysts numerically modelling fluid flow problems, a regime usually suited for the Finite Difference or Finite Volume approaches.

2.2.1.2 The Finite Difference Method.

The Finite Difference (FD) approach is frequently included in analyses that involve time dependent results, and also in numerical solutions that require problem-specific attention. The FD approach, unlike the FE approach, is one that is usually specifically formulated for a distinct family of numerical problems. This requires the analyst to intimately understand the finite difference approximation of the governing differential equations utilized in his or her approach.

$$u_{t+1,k} - \frac{v_o \Delta t}{2\Delta x^2} (u_{t+1,k+1} - 2u_{t+1,k} + u_{t+1,k-1}) = u_{t,k} + \frac{v_o \Delta t}{2\Delta x^2} (u_{t,k+1} - 2u_{t,k} + u_{t,k-1}) \quad (2.2)$$

The Crank-Nicolson scheme, shown in equation 2.2 in one dimension, is an example of a FD approximation. Here u is the variable of interest, v_o is a constant, t is time, and x and k are space (Thomas, 1995). This FD method has been further refined to include a class of fluid dynamic problems, commonly referred to as the Finite Volume method.

2.2.1.3 The Finite Volume Method.

The Finite Volume (FV) approach is a popular choice of formulation for the advection and diffusion of heat and material. The FV approach usually considered a subset of the Finite Difference method. Scientists studying flow phenomenon such as aerodynamics and hydrodynamics may choose this approach. Compressible and

incompressible fluid flow regimes are examples of problems that might be modeled in a FV approach. equation 2.3, below, is an example of a steady-state finite volume approximation for incompressible convection/ diffusion in one dimension, where u is the variable of interest, v is velocity, λ_o and ρ_o are constants, x and k are space (Patankar, 1980).

$$\left(\frac{\lambda_o}{\Delta x_{k+1}} + \frac{\lambda_o}{\Delta x_{k-1}} + \frac{\rho_o v_{k+1}}{2} - \frac{\rho_o v_{k-1}}{2} \right) u_k = \left(\frac{\lambda_o}{\Delta x_{k+1}} - \frac{\rho_o v_{k+1}}{2} \right) u_{k+1} + \left(\frac{\lambda_o}{\Delta x_{k-1}} + \frac{\rho_o v_{k-1}}{2} \right) u_{k-1} \quad (2.3)$$

This equation, equation 2.3, is in reality a specialized version of the Crank-Nicolson scheme shown in equation 2.2, applied specifically to incompressible, steady-state convection and diffusion.

The selection of one or more of these modeling approaches largely depends of the analysis problem. Each of these numerical techniques have been exhaustively studied and characterized. One can read from decades of findings published on the results of various numerical methods, or combinations of methods for specific applications.

2.2.2 Lagrangian and Eulerian Techniques

The Finite Element, Finite Difference, and Finite Volume numerical modeling approaches fall into two main categories or techniques, namely Lagrangian and Eulerian. In a Lagrangian approach the domain is divided into nodal points and elements that distort and travel with the deforming material. In an Eulerian

formulation of a numerical problem, the domain is again divided into nodal points and elements, with these points and elements remaining constant during the analysis. Thus, the deforming material flows through the domain. (See Figure 2.1.)

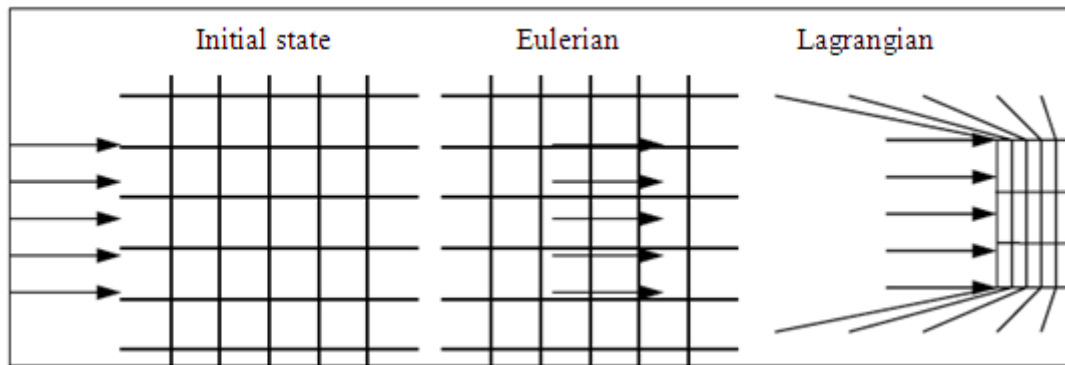


Figure 2.1 : Eulerian and Lagrangian approaches to numerical modelling. Notice the material moves through the Eulerian mesh, and distorts the Lagrangian mesh (Oliphant, 2004).

2.2.2.1 The Lagrangian Approach.

Both Lagrangian and Eulerian methods provide benefits and introduce challenges. The Lagrangian formulation tends to return highly accurate results, void of numerical dispersion, or the creation of false data. However, Lagrangian schemes only work well for low deformation problems. (High deformation problems tend to invert and tangle the meshed domain.) Therefore, if a researcher desires to use a Lagrangian scheme for high deformation problems, he must, as the problem progresses, employ a method of remapping, or remeshing his domain and transferring the material deformation information to the new domain.

2.2.2.2 The Eulerian Approach.

Eulerian approaches bypass this challenge of the Lagrangian schemes by simply keeping the meshed domain constant, and allowing the material to flow through the mesh. Thus, Eulerian formulations handle high deformation of materials quite easily. Challenging the user, however, is the presence of numerical dispersion. (Refining the mesh size sufficiently to remove the problem, or implementing a second order accurate solution reduces the effects of numerical dispersion.)

2.2.2.3 The Arbitrary Lagrangian Eulerian Approach

Coupling the two approaches seems to be the most viable option for modelling events that require zones of high material deformation, while other areas of the problem tend to remain in a semi-stationary fashion. There is a recently growing approach to modeling that combines the Lagrangian and Eulerian methods into a single numerical approach, the Arbitrary Lagrangian Eulerian (ALE) method. In this approach, a modeler specifies a set of metrics that informs the analysis code when to use a Lagrangian approach, or an Eulerian approach. These metrics may include element volume, skew, temperature, or other similar properties.

Previous friction welding researchers have applied various combinations of the Finite Element, Finite Difference, and Finite Volume approaches to model the FW process. These approaches have been implemented in Lagrangian, Eulerian, and ALE formulations, each with strengths and weaknesses. Several researchers have approached the process with a fully three dimensional domain, while others have

elected to focus on a two dimensional simplification of the geometry. Each of these modeling attempts incorporates simplifying assumptions for the weld material, the frictional contact interface, and the geometry. Therefore, the principal motivation for this research was to capture the friction welding process as accurately as possible by reducing the number of simplifying assumptions utilized in the modelling process.

2.3 Modelling the FW Process

Models are important in the drive to move away from a trial and error approach to optimizing weld process parameters, whether that be to obtain a given upset, optimize the microstructure, or to control residual stresses. Weld process modellers have generally moved away from explicitly modelling the complete rotational welding process due to the computational demands associated with such a task. This is because of the very severe circumferential strains that are introduced in the narrow weld region. Instead researchers have tended to neglect the rotational motion itself, preferring to capture indirectly the effects of the high rate of straining and the extensive shearing that it causes at, or near, the contact surfaces. As a result, most models regard rotational welding largely as a forging together of two axisymmetric materials where the heating, and the resulting local plastic properties, are determined by the rate at which rotational energy or work is transferred to the workpieces. In other words the rate at which heat is generated has been calculated in terms of the work done by the motor in direct drive rotational friction welding (DD-RFW), or the rate of change of the kinetic energy of the flywheel in the case of inertia friction welding (IFW).

As mentioned above, when IFW components the operator has relatively little direct control over the upset, thermal evolution and welding time compared to direct drive processes. As a result in order to achieve a specified upset, weld microstructure and residual stresses the welding engineer either has to rely on a matrix of welding trials varying the initial angular velocity, flywheel momentum and pressure in order to arrive at the desired result by trial and error, or have access to a weld process model that provides the link between them. Considering the inertia welding of aeroengine assemblies (Preuss et al., 2002, Karadge et al., 2011) for example, dimensional tolerances of 100 μ m are required in order that the assembled engine is within specification, while a high level of control over microstructure and residual stress is also desirable. This places tremendous requirements on the control and repeatability of the inertia welding process. Furthermore, a trial and error approach would be simply too expensive on full-scale assemblies, while the extrapolation of process parameters from sub-scale prototype testing would not be feasible. Consequently, inertia friction weld models are of great importance commercially.

2.4 Realistic friction law for FW model

An important aspect when modelling is the adoption of suitable constitutive laws by which materials behaviour can be represented. DD-RFW is characterised by strain rates reaching 1000 s⁻¹ locally (Midling and Grong, 1994). As a result, the strain rate dependency of the stress-strain response (e.g. Figure 2.2a) must be captured by reliable constitutive equations.

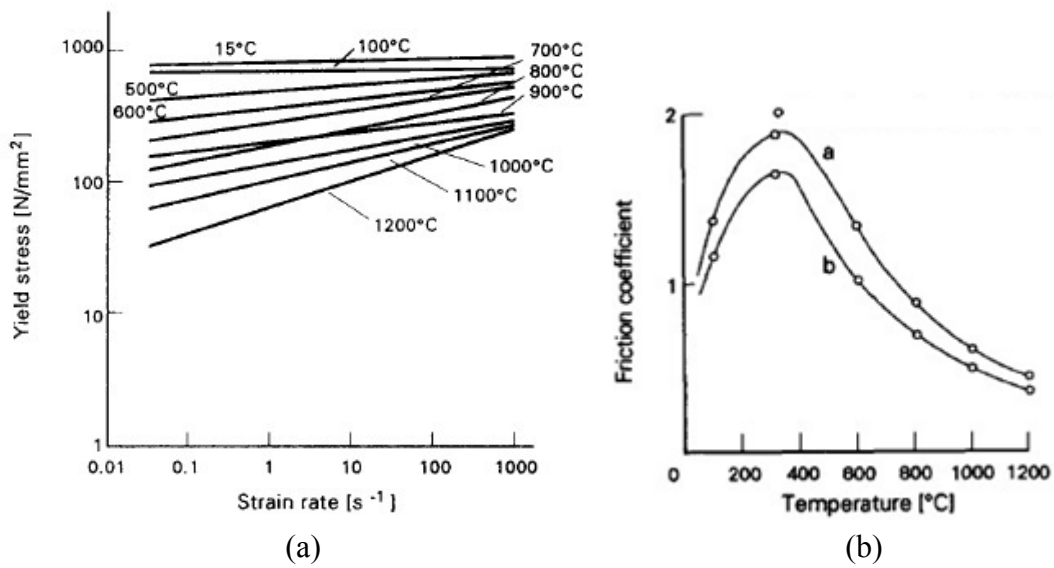


Figure 2.2: a) Yield stress of 20G steel as a function of strain rate, b) Friction coefficient as a function of temperature at two pressures (a: 40 N/mm²; b: 60 N/mm²). The continuous lines denote the relation used for the numerical simulation in section 2.4 (Sluzalec, 1990).

Equally important is the effective ‘friction’ response. Friction has been treated in modeling strategies in a number of ways. Early work involved the assumption that the friction coefficient, μ_{fr} , is either constant or varies radially (Hollander, 1962, Vill, 1962). However, it is typically pressure, P , temperature, T , and sliding speed, v , sensitive (Figure 2.2b). When modelling inertia friction welding nickel-base superalloys, Moal et al. (1992) did not consider the effect of temperature on friction behaviour explicitly as in Figure 2.2b, but rather simply plotted the change in τ/P as a function of angular velocity. Balasubramanian et al. (1999b) undertook a combined experimental and theoretical analysis of steel DD-RFW to try and derive an appropriate ‘friction’ law by fitting numerical models to measured thermal profiles. Using a regression analysis for 1045 steels they obtained the relation: